

# Fano line shape metamorphosis in resonant two-photon ionization

Vladislav V. Serov<sup>1</sup> and Anatoli S. Kheifets<sup>2</sup>

<sup>1</sup>*General, Theoretical and Computer Physics, Saratov State University, Saratov 410012, Russia and*

<sup>2</sup>*Research School of Physics, The Australian National University, Canberra ACT 2601, Australia\**

(Dated: May 29, 2024)

Two-photon atomic ionization driven by time-locked XUV and IR pulses allows to study dynamics of Fano resonances in time and energy domains. Different time evolution of the two interfering pathways leading to a Fano resonance can be exploited to turn the Fano profile of the two-photon XUV/IR ionization into a symmetric Gaussian once the directly ejected photoelectron leaves the parent ion and cannot any longer absorb an IR photon. This line shape transformation allows for the direct determination of the resonant lifetime from the spectroscopic measurements without need for an extremely fine energy resolution. Ubiquitous nature of Fano resonances makes this determination a universal tool in diverse quantum systems ranging from nuclei to nano-fabricated solids.

PACS numbers: 32.80.Rm 32.80.Fb 42.50.Hz

Ugo Fano's most enduring legacy in atomic physics is his theory of Bound states embedded Into Continuum (BIC) [1–3]. Fano's theory explained an earlier [4] and stimulated subsequent [5] measurements which detected distinctive asymmetric line shapes in atomic ionization cross-sections. The cross-section near the Fano resonance takes the form

$$\sigma(\epsilon) = |D(\epsilon)|^2 \propto \frac{(\epsilon + q)^2}{\epsilon^2 + 1}, \quad \epsilon = \frac{E - E_0}{\Gamma/2}. \quad (1)$$

Here  $\epsilon$  is a detuning from the resonance center  $E_0$  measured in units of the resonance half width and  $q$  is the Fano shape index. The ionization amplitude in Eq. (1) can be expressed via the phases of the resonant and non-resonant (background) scattering [6]:

$$D(\epsilon) \propto [e^{2i(\delta+\phi)} - 1]/2, \quad \cot \delta = \epsilon, \quad \cot \phi = q \quad (2)$$

In the absence of the background scattering when  $\phi = 0$  the Fano profile turns into a Lorentzian which is characteristic for an exponential decay of a discrete excited state with a finite lifetime  $\tau = 1/\Gamma$  [7].

The BIC phenomenon is ubiquitous in nature. In recent decades, Fano resonances have been observed in very diverse systems such as Mössbauer nuclei [8], quantum dots [9], plasmonic nanostructures [10–12], 2D photonic crystals [13], metasurfaces [14] and exploited widely in nanotechnology and nanophotonics [15–18].

In atomic physics, a renewed interest to Fano resonances has been stimulated by availability of ultra-short laser pulses. These novel laser sources have allowed to study ultrafast dynamics of Fano resonances both in the time and energy domains [19–27]. Not only can the Fano resonances be probed with lasers. Intense laser pulses have the capacity to induce a coupling of a resonant state to the continuum which otherwise does not naturally occur [28]. Lasers can also blur the difference between the

Fano and Lorentz line shapes [19]. The photoelectron continuum phase  $\phi$  can be offset by a ponderomotive energy kick from a strong IR pulse. Such a compensation turns a Fano photoabsorption line into a Lorentzian.

Even though autoionizing two-electron excitations in He were discovered nearly a century ago [29], their studies still remain a very active research area, i.e. [30–32]. Time resolution of the Fano resonances sheds new light on this phenomenon by providing a universal phase control [19, 21] and monitoring the birth of a photoelectron [20, 22]. However, there is little direct overlap between the old and new physics of Fano resonances. Majority of time resolved studies of Fano resonances have been conducted using the technique of Reconstruction of Attosecond Beating By Interference of Two-photon Transitions (RABBITT) [20, 23–27]. Even though resonant  $r$ RABBITT method can scan the photoelectron spectral lines with a sufficient resolution, these lines remain too broad for direct spectroscopic determination of the accurate resonance position and width. This become particularly problematic for highly excited and narrow resonant states. Neither can the Fano shape index be measured directly from photoelectron line shapes. The bound state structure of the target can be deduced from an under-threshold  $u$ RABBITT process [27, 33–36]. However, this determination is restricted to single-electron excitations below the ionization threshold.

In the RABBITT technique, an atom is ionized by an XUV pump in the form of an attosecond pulse train (APT). The corresponding photoelectron spectrum contains a comb of primary harmonic peaks centering at the odd multiples of the IR probe frequency  $\Omega_{2q\pm 1} = (2q \pm 1)\omega$ . Arrival of an IR probe adds new spectral features known as sidebands (SB's). They correspond to an even frequency  $\Omega_{2q} = 2q\omega$  and are formed by the two competing pathways  $\Omega_{2q+1} - \omega$  and  $\Omega_{2q-1} + \omega$ . These two pathways interfere and the SB population oscillates as the XUV/IR delay  $\Delta$  varies:

$$S_{\text{SB}}(\Delta) \propto b \cos[2\omega\Delta - \delta], \quad \delta = 2\omega\tau_a. \quad (3)$$

The magnitude  $b$  and phase  $\delta$  of the RABBITT oscilla-

\*Electronic address: A.Kheifets@anu.edu.au

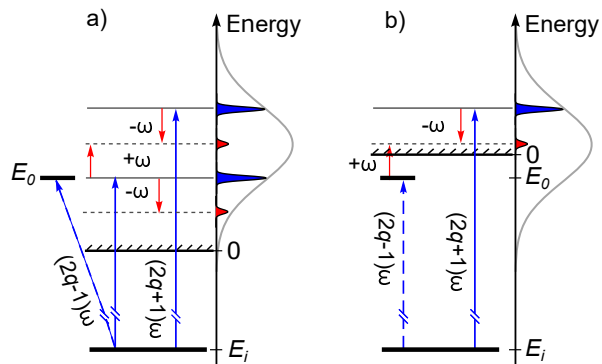


FIG. 1: Schematic representation of the resonant  $r$ RABBITT (a) and the under-threshold  $u$ RABBITT (b) processes. Direct and resonant XUV absorption pathways are shown with solid and dashed lines, respectively.

tions can be expressed via two-photon ionization amplitudes [37]. The RABBITT phase can then be converted to the atomic time delay  $\tau_a = \delta/(2\omega)$ .

In the resonant  $r$ RABBITT process, one of the main odd harmonics is tuned to an autoionization resonance as shown in Fig. 1a. In this case, the RABBITT parameters of the two neighboring SBs display a clear resonant structure. In the underthreshold  $u$ RABBITT process illustrated graphically in Fig. 1b, the discrete excited state is located below the threshold and only the lowest SB is affected by the resonance. In principle, an  $r$ RABBITT measurement can detect the lifetime of the resonance. However, because of the  $2\omega$  periodicity in Eq. (3), the useful range of the XUV/IR delays is restricted to the half cycle of the IR oscillation which is 2.6 fs for the commonly used 800 nm wavelength. This range is far too narrow for majority of atomic and molecular autoionizing resonances.

In the present work, we remove this restriction by employing an isolated XUV pulse instead of an APT. We assume that the duration of the XUV pulse is much shorter than the lifetime of the autoionizing state  $\tau$ . In the meantime, its spectral width is smaller than  $\omega$  such that SB's are well separated from the main photoelectron line. We consider an IR pulse of the duration  $T$  with a Gaussian envelope

$$E(t) = f(t) \sin[\omega(t - \Delta)], \quad f(t) = \exp\left[-\frac{(t - t_0)^2}{2T^2}\right]. \quad (4)$$

Arrival of the IR pulse populates the two SB's centered at  $E_0 \pm \omega$ . The SB amplitude is obtained by a simple Fourier transform

$$A_{\text{SB}}(\varepsilon) \sim \int_0^\infty \exp\left[i\varepsilon t - \frac{(t - t_0)^2}{2T^2} - \frac{t}{2\tau}\right] dt, \quad (5)$$

where  $\varepsilon$  is the absolute detuning from the center of the SB. The integration in Eq. (5) is carried out from the moment of arrival of the XUV pulse at  $t = 0$ , when the autoionizing state is instantly (compared to  $T$  and  $\tau$ )

populated. The integration results in

$$A_{\text{SB}}(\varepsilon) \sim \exp\left[-\frac{T^2(2i\varepsilon\tau - 1)^2}{8\tau^2} - i\varepsilon t_0 - \frac{t_0}{2\tau}\right] \times \left[\text{erf}\left\{\frac{T(2i\varepsilon\tau - 1)}{\sqrt{8\tau}} + \frac{t_0}{\sqrt{2T}}\right\} + 1\right]. \quad (6)$$

At  $t_0 \gg T$  the SB acquires a Gaussian line shape

$$S_{\text{SB}}(\varepsilon) = |A_{\text{SB}}(\varepsilon)|^2 \sim \exp\left[-T^2\varepsilon^2 - \frac{t_0}{\tau}\right] \quad (7)$$

The width of the Gaussian is determined by the length of the IR pulse  $T$  but not the width of the resonance  $\Gamma$ . The magnitude of the Gaussian decreases exponentially with increasing  $t_0$ . The timing constant of this exponential decay is equal to the lifetime of the autoionizing state  $\tau$ .

Qualitatively, the line shape (6) is easy to understand. The IR pulse ejects into the continuum a number of electrons proportional to the population the autoionizing state at the moment of its arrival. If  $t_0 = 0$  and  $T \gg \tau$ , the distribution (6) becomes a Lorentzian

$$|S_{\text{SB}}(\varepsilon)|^2 \sim (\varepsilon^2 + \tau^2/4)^{-1} \quad (8)$$

In addition to exciting an autoionizing state (resonant excitation, dashed line in Fig. 1a), the XUV pulse causes the direct ionization (solid line in the same figure). Thus the resonant SB amplitude is the sum of the two terms

$$A_{\text{SB}}(\varepsilon) = A_{\text{SB,R}}(\varepsilon) + A_{\text{SB,CC}}(\varepsilon). \quad (9)$$

Here  $A_{\text{SB,CC}}(\varepsilon)$  is the amplitude of the continuum-continuum transition in the IR field. At  $t_0 = 0$ , this amplitude has a magnitude comparable to  $A_{\text{SB,R}}(\varepsilon)$ , so their summation leads to an asymmetric line shape similar to the Fano profile. The wave packet of electrons ejected directly by the XUV pulse moves away from the ion as  $t$  grows. At sufficiently long XUV/IR delay  $t_0 \rightarrow \infty$ , the IR pulse will not alter the energy of the photoelectron. Classically, a free electron cannot absorb a photon to conserve both the momentum and energy. Hence, in the case of a large XUV/IR delay,  $A_{\text{SB,CC}}(\varepsilon, t_0 \rightarrow \infty) \rightarrow 0$  so that the SBs acquire a symmetric Gaussian line shape.

This simple analytical model is supported by accurate numerical simulations in two-electron targets, the He atom and the  $\text{Li}^+$  ion. In these simulations, we solve numerically the time-dependent Schrödinger equation (TDSE) on a multi-configuration basis as described in detail in [38]. To test and validate our numerical technique, we first conduct the  $r$ RABBITT calculation on He and make a comparison with experimental and theoretical results presented in an earlier work [24]. This comparison is shown in Fig. 2. Here we display the RABBITT magnitude  $b$  and phase  $\delta$  parameters in Eq. (3) for SB38 and SB40 when the harmonic H39 is tuned to the  $sp2^+$  resonance. The perturbation theory calculation in [24] and the present numerical results sandwich the experimental data sufficiently closely. From this we

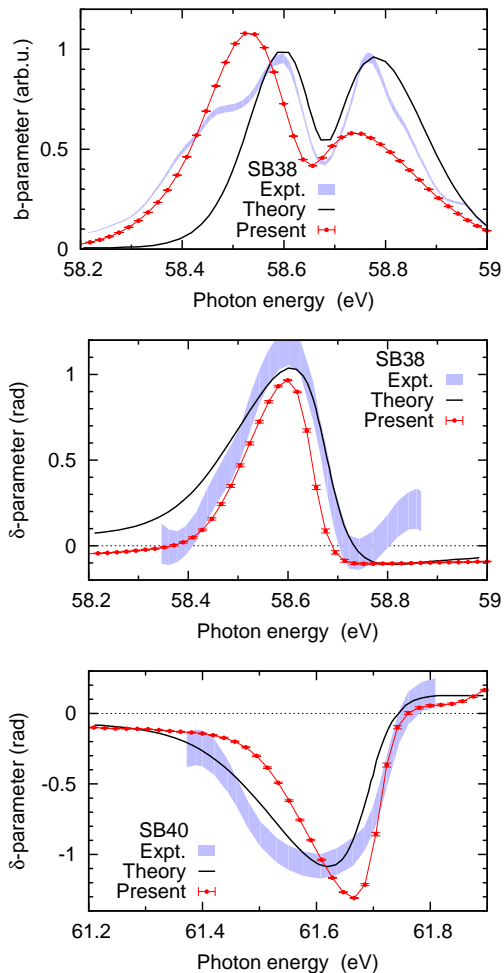


FIG. 2:  $r$ RABBITT magnitude and phase parameters in He when H39 is tuned to the  $sp2^+$  resonance. Top: the magnitude  $b$  parameter of SB38. Middle and bottom: the phase  $\delta$  parameters of SB38 and SB40, respectively. The experimental and theoretical results of [24] are compared with the present calculation. The error bars in the latter indicate the accuracy of the fit with Eq. (3).

can conclude that our numerical accuracy is at least not worse than that in the previous work [24].

Once our numerical method is tested and validated, we return to the core problem of the present investigation. To do so, we substitute the APT in  $r$ RABBITT with an isolated XUV pulse. In addition, we shorten the duration of the IR pulse from 21 fs in RABBITT simulations to 7 fs in the Fano line shape study. We consider the same lowest two-electron excitation  $sp2^+$  in He. Of all the helium autoionizing states, this resonance has the shortest lifetime of 17 fs which corresponds to  $\Gamma = 36$  meV [39]. This resonance was not considered in [19] because the IR pulse could couple it strongly with non-dipole  $2p^2$  excitations [40, 41]. We eliminate this complication by tripling the energy of the IR photon from 1.55 eV (800 nm) as in [24] to 4.6 eV (266 nm).

The graphical illustration of our numerical results is

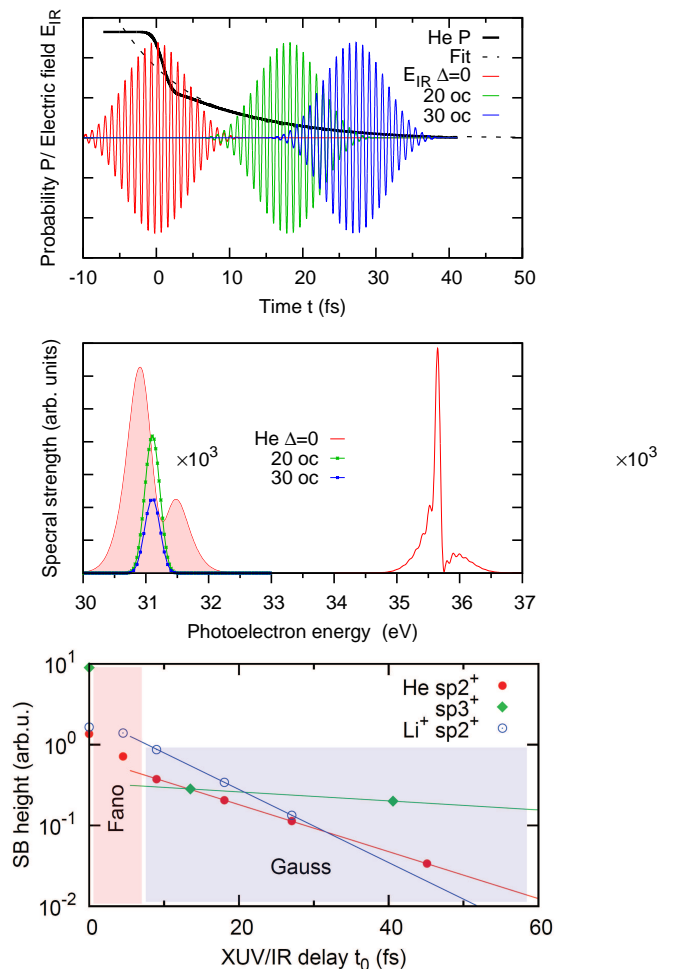


FIG. 3: Top: the thick solid line shows the scaled probability of locating the departing photoelectron within the simulation boundary. Differently colored IR probes arrive at various delays (in units of optical cycles, 1 oc=0.9 fs). Middle: the photoelectron spectrum corresponding different XUV/IR delays. The SBs (only one set is shown) are scaled by a factor  $10^3$  for better visibility. Bottom: the SB height as a function of the XUV/IR delay is fitted with an exponential decay function. The shaded areas mark the Fano and Gauss line shape appearance. The top and middle panels display the He  $sp2^+$  data whereas the bottom panel shows the He  $sp2^+$ ,  $sp3^+$  and  $Li^+ sp2^+$  data.

shown in Fig. 3. The XUV probe arrives at the time zero and sets in motion the photoelectron which leaks outside the simulation boundary. The thick solid line in the top panel of the figure shows the probability of finding the photoelectron inside this boundary. Once this probability decreases with time, the IR probe pulse arrives at variable delay. This probe adds two SBs to the main peak in the photoelectron spectrum. Only one set of SB's is shown in the middle panel of the figure for better clarity. The main peak exhibits a typical asymmetric Fano line shape irrespective of the XUV/IR delay. When the XUV pump and IR probe overlap, the SBs

display similar asymmetric line shapes. As the XUV/IR delay  $\Delta$  grows and the photoelectron population inside the boundary starts to decrease, this asymmetry of the SB vanishes and the resonance decays exponentially as prescribed by Eq. (6). From this point on, by monitoring the SB height, we can deduce the lifetime of the resonance. This procedure is illustrated in the bottom panel of the figure where the SB height is fitted with an exponential decay function  $\propto \exp(-\Delta/\tau)$ . The lifetime of the resonance  $\tau = 15$  fs found this way is rather close to the experimental value of 17 fs [39]. We repeat this determination for other autoionizing states. For the  $sp3^+$  resonance of He, we need not increase the IR frequency as it does not mix with other autoionizing states. Our determination returns the lifetime values of 81.7 fs (upper SB) and 79.5 fs (lower SB). This is to compare with the experimental value of 82 fs [39]. The  $sp2^+$  resonance in  $Li^+$  ion has the line width of 74 meV and the corresponding life time of 8.7 fs [42]. Our determination as illustrated in the bottom panel of Fig. 3 returns  $\tau = 9.6$  fs.

Incidentally, the exponential decay fit of the autoionizing state population as shown in the top panel of Fig. 3 returns identical  $\tau$  values for both targets. So the difference between the theoretical and experimental lifetimes is due to deficiency of the theoretical description of the resonance with a limited number of configurations. The exponential fitting of the SB's does not introduce any error and once applied in experiment will return the accurate lifetime.

In conclusion, we study ultrafast dynamics of the autoionizing states in two-electron atomic targets driven by a combination of an ionizing XUV pump pulse and a delayed and weak IR probe pulse. The two-photon ionization manifests itself by appearance of sidebands displaced from the main photoelectron line by the energy of the IR photon. When the XUV pump is tuned to the resonance, the main peak in the photoelectron spectrum acquires a characteristic asymmetric Fano line shape. In the meantime, the shape of the sidebands varies depending on the XUV/IR delay. When this delay is sufficiently large and

the directly ionized electron leaves the parent ion, the Fano line shape of the sidebands turns into a symmetric Gaussian. In this regime, a free electron cannot absorb an IR photon and the direct pathway cannot compete with its resonant counterpart. As the XUV/IR delay is increased further, evolution of the SB height becomes particularly simple and can be represented by an exponential decay function. The use of this function allows for an accurate determination of the lifetime of the resonance. This behavior is predicted analytically and further supported by accurate numerical simulations. Even though the presented calculations are performed for atomic targets, our development of the molecular TDSE code [38] allows for similar simulations in molecules such as  $H_2$ .

The proposed determination of the resonant life time does not require an extremely fine spectral resolution. It is sufficient for this determination that the SB height decreases with XUV/IR delay while the resonance is not fully spectrally resolved. This is particularly beneficial for studying highly excited and long living autoionizing states in atoms and molecules while the photoelectron energy resolution is modest. This is in contrast to other spectroscopic techniques. For instance, transient photoabsorption spectroscopy of the He autoionizing states with a lifetime exceeding 100 fs requires a spectral resolution better than 20 meV [19]. The more severe case is a Mössbauer nuclei which exhibits resonances with lifetime exceeding 100 ns and the spectral width of the order of neV [8]. For such narrow resonances the proposed technique could be particularly beneficial since its accuracy grows for longer lifetimes exceeding duration of the probe pulse. Because Fano resonances are so prevalent in nature, we expect a wide application of the proposed method. The spectral range of the pump and probe pulses can vary from THz radiation in semiconductors [28] to  $\gamma$ -rays in nuclei [8]. Nevertheless, the basic principle of the proposed technique remains the same.

*Acknowledgment:* This work was supported by the Discovery Grant DP190101145 from the Australian Research Council.

- 
- [1] U. Fano, *On the absorption spectrum of noble gases near the limit of the arc spectrum*, Nuovo Cimento **12**, 154–161 (1935).
- [2] U. Fano, *Effects of configuration interaction on intensities and phase shifts*, Phys. Rev. **124**, 1866 (1961).
- [3] U. Fano and J. W. Cooper, *Line profiles in the far-uv absorption spectra of the rare gases*, Phys. Rev. **137**, A1364 (1965).
- [4] S. M. Silverman and E. N. Lassettre, *Additional Collision Cross Sections for Helium Especially in the Ionized Continuum*, J. Chem. Phys. **40**(5), 1265 (1964).
- [5] R. P. Madden and K. Codling, *New autoionizing atomic energy levels in He, Ne, and Ar*, Phys. Rev. Lett. **10**, 516 (1963).
- [6] J. P. Connerade and A. M. Lane, *Interacting resonances in atomic spectroscopy*, Rep. Progr. Phys. **51**(11), 1439 (1988).
- [7] H. A. Lorentz, *The theory of electrons and its applications to the phenomena of light and radiant heat* (B.G. Teubner, Leipzig, 1916).
- [8] T.-J. Li, X.-C. Huang, Z.-R. Ma, B. Li, X.-Y. Wang, and L.-F. Zhu, *Fano-Lorentz shape controlled by the collective effect of the nuclear ensemble*, Phys. Rev. A **108**, 033715 (2023).
- [9] M. Kroner, A. O. Govorov, S. Remi, B. Biedermann, S. Seidl, A. Badolato, P. M. Petroff, W. Zhang, R. Barbour, B. D. Gerardot, et al., *The nonlinear Fano effect*, Nature **451**, 311 (2008).
- [10] J. A. Fan, C. Wu, K. Bao, J. Bao, R. Bardhan, N. J. Halas, V. N. Manoharan, P. Nordlander, G. Shvets, and F. Capasso, *Self-assembled plasmonic nanoparticle clusters*, Science **328**(5982), 1135 (2010).

- [11] B. Luk'yanchuk, N. I. Zheludev, S. A. Maier, N. J. Halas, P. Nordlander, H. Giessen, and C. T. Chong, *The Fano resonance in plasmonic nanostructures and metamaterials*, *Nature Materials* **9**, 707 (2010).
- [12] M. Rahmani, B. Luk'yanchuk, and H. Minghui, *Fano resonance in novel plasmonic nanostructures*, *Laser & Photonics Reviews* **7**(3), 329 (2012).
- [13] W. Zhou, D. Zhao, Y.-C. Shuai, H. Yang, S. Chuwongin, A. Chadha, J.-H. Seo, K. X. Wang, V. Liu, Z. Ma, et al., *Progress in 2D photonic crystal Fano resonance photonics*, *Progress in Quantum Electronics* **38**(1), 1 (2014).
- [14] Y. Yang, W. Wang, A. Boulesbaa, I. I. Kravchenko, D. P. Briggs, A. Poretzky, D. Geohegan, and J. Valentine, *Nonlinear Fano-resonant dielectric metasurfaces*, *Nano Letters* **15**, 7388 (2015).
- [15] A. E. Miroshnichenko, S. Flach, and Y. S. Kivshar, *Fano resonances in nanoscale structures*, *Rev. Mod. Phys.* **82**, 2257 (2010).
- [16] C. W. Hsu, B. Zhen, A. D. Stone, J. D. Joannopoulos, and M. Soljacić, *Bound states in the continuum*, *Nature Reviews Materials* **1**, 16048 (2016).
- [17] M. F. Limonov, M. V. Rybin, A. N. Poddubny, and Y. S. Kivshar, *Fano resonances in photonics*, *Nature Photonics* **11**, 543 (2017).
- [18] K. L. Koshelev, Z. F. Sadrieva, A. A. Shcherbakov, Y. S. Kivshar, and A. A. Bogdanov, *Bound states in the continuum in photonic structures*, *Phys. Usp.* **66**(5), 494 (2023).
- [19] C. Ott, A. Kaldun, P. Raith, K. Meyer, M. Laux, J. Evers, C. H. Keitel, C. H. Greene, and T. Pfeifer, *Lorentz meets Fano in spectral line shapes: A universal phase and its laser control*, *Science* **340**(6133), 716 (2013).
- [20] V. Gruson, L. Barreau, Á. Jiménez-Galan, F. Risoud, J. Caillat, A. Maquet, B. Carré, F. Lepetit, J.-F. Hergott, T. Ruchon, et al., *Attosecond dynamics through a Fano resonance: Monitoring the birth of a photoelectron*, *Science* **354**(6313), 734 (2016).
- [21] M. Kotur, D. Guénot, Jiménez-Galán, D. Kroon, E. W. Larsen, M. Louisy, S. Bengtsson, M. Miranda, J. Mauritsson, C. L. Arnold, et al., *Spectral phase measurement of a Fano resonance using tunable attosecond pulses*, *Nature Communications* **7**, 10566 (2016).
- [22] A. Kaldun, A. Blättermann, V. Stooss, S. Donsa, H. Wei, R. Pazourek, S. Nagele, C. Ott, C. D. Lin, J. Burgdörfer, et al., *Observing the ultrafast buildup of a Fano resonance in the time domain*, *Science* **354**(6313), 738 (2016).
- [23] C. Cirelli, C. Marante, S. Heuser, C. L. M. Petersson, A. J. Galán, L. Argenti, S. Zhong, D. Busto, M. Isinger, S. Nandi, et al., *Anisotropic photoemission time delays close to a Fano resonance*, *Nature Comm.* **9**, 955 (2018).
- [24] D. Busto, L. Barreau, M. Isinger, M. Turconi, C. Alexandridi, A. Harth, S. Zhong, R. J. Squibb, D. Kroon, S. Plogmaker, et al., *Time-frequency representation of autoionization dynamics in helium*, *J. Phys. B* **51**(4), 044002 (2018).
- [25] L. Barreau, C. L. M. Petersson, M. Klinker, A. Camper, C. Marante, T. Gorman, D. Kieseewetter, L. Argenti, P. Agostini, J. González-Vázquez, et al., *Disentangling spectral phases of interfering autoionizing states from attosecond interferometric measurements*, *Phys. Rev. Lett.* **122**, 253203 (2019).
- [26] M. Turconi, L. Barreau, D. Busto, M. Isinger, C. Alexandridi, A. Harth, R. J. Squibb, D. Kroon, C. L. Arnold, R. Feifel, et al., *Spin-orbit-resolved spectral phase measurements around a fano resonance*, *J. Phys. B* **53**(18), 184003 (2020).
- [27] L. Neoricic, D. Busto, H. Laurell, R. Weissenbilder, M. Ammitzböll, S. Luo, J. Peschel, H. Wikmark, J. Lahl, S. Maclot, et al., *Resonant two-photon ionization of helium atoms studied by attosecond interferometry*, *Frontiers in Physics* **10** (2022).
- [28] K. L. Litvinenko, N. H. Le, B. Redlich, C. R. Pidgeon, N. V. Abrosimov, Y. Andreev, Z. Huang, and B. N. Murrin, *The multi-photon induced Fano effect*, *Nature Communications* **12**, 454 (2021).
- [29] K. Compton and J. Boyce, *Extreme ultraviolet spectra excited by controlled electron impacts*, *J. Franklin Inst.* **205**(4), 497 (1928).
- [30] C. Lin, *Doubly excited states, including new classification schemes*, *Adv. At. Mol. Phys.* **22**, 77 (1986).
- [31] J. M. Rost, K. Schulz, M. Domke, and G. Kaindl, *Resonance parameters of photo doubly excited helium*, *J. Phys. B* **30**(21), 4663 (1997).
- [32] L. Argenti, *Rydberg and autoionizing triplet states in helium up to the  $N = 5$  threshold*, *Atomic Data and Nuclear Data Tables* **94**(6), 903 (2008).
- [33] M. Swoboda, T. Fordell, K. Klünder, J. M. Dahlström, M. Miranda, C. Buth, K. J. Schafer, J. Mauritsson, A. L'Huillier, and M. Gisselbrecht, *Phase measurement of resonant two-photon ionization in helium*, *Phys. Rev. Lett.* **104**, 103003 (2010).
- [34] D. M. Villeneuve, P. Hockett, M. J. J. Vrakking, and H. Niikura, *Coherent imaging of an attosecond electron wave packet*, *Science* **356**(6343), 1150 (2017).
- [35] A. S. Kheifets and A. W. Bray, *RABBITT phase transition across the ionization threshold*, *Phys. Rev. A* **103**, L011101 (2021).
- [36] A. Kheifets, *Revealing the target electronic structure with under-threshold RABBITT*, *Atoms* **9**(3), 66 (2021).
- [37] J. M. Dahlström et al., *Theory of attosecond delays in laser-assisted photoionization*, *Chem. Phys.* **414**, 53 (2013).
- [38] V. Serov, *Time-dependent convergent close coupling method for molecular ionization in laser fields* (2024), arXiv:2405.12455.
- [39] M. Domke, K. Schulz, G. Remmers, G. Kaindl, and D. Wintgen, *High-resolution study of  $1P^o$  double-excitation states in helium*, *Phys. Rev. A* **53**, 1424 (1996).
- [40] Z.-H. Loh, C. H. Greene, and S. R. Leone, *Femtosecond induced transparency and absorption in the extreme ultraviolet by coherent coupling of the He  $2s2p(1P^o)$  and  $2p^2(1S^e)$  double excitation states with 800nm light*, *Chem. Phys.* **350**(1), 7 (2008).
- [41] W.-C. Chu, S.-F. Zhao, and C. D. Lin, *Laser-assisted autoionization dynamics of helium resonances with single attosecond pulses*, *Phys. Rev. A* **84**, 033426 (2011).
- [42] P. K. Carroll and E. T. Kennedy, *Doubly excited autoionization resonances in the absorption spectrum of  $Li^+$  formed in a laser-produced plasma*, *Phys. Rev. Lett.* **38**, 1068 (1977).